Article

An Electrogenerated Chemiluminescence Biosensor using a tripod probe for the Highly Sensitive Detection of MicroRNA

Liping Lu, Jiaxing Wang, Wujian Miao, Xiayan Wang, and Guangsheng Guo

Anal. Chem., **Just Accepted Manuscript** • DOI: 10.1021/acs.analchem.8b04271 • Publication Date (Web): 19 Dec 2018

An Electrogenerated Chemiluminescence Biosensor using a tripod probe for the Highly Sensitive Detection of MicroRNA

Liping Lu[†]*, Jiaxing Wang[†], Wujian Miao[‡]*,
Xiayan Wang[†], Guangsheng Guo[†]

[†] College of Environmental and Energy Engineering, Beijing University of Technology, Beijing 100124, China
[‡] Department of Chemistry and Biochemistry, The University of Southern Mississippi, Hattiesburg, MS 39406

***E-mail addresses: lipinglu@bjut.edu.cn ; wujian.miao@usm.edu**

ABSTRACT

A novel probe for highly sensitive detection of microRNA, that enhanced the helix accessibility and yielded good assembling without backfilling, was developed using a tripod structure fabricated by triplex DNA. A layer of triplex DNA assembled on electrodeposited reduced graphene oxide was used as the capture probe and a subsequent hybridization chain reaction that promoted the efficient intercalation of the electrogenerated chemiluminescence(ECL) emitter $[Ru(bpy)_2(dppz)]^{2+}$ (bpy = 2,2′-bipyridine, dppz = dipyrido[3,2-*a*: 2′,3′-*c*]phenazine) was used an analytical signal amplifier. The fabricated biosensor was examined with an anodic ECL mode using tri-*n*-propyl amine as the coreactant. The construction of the biosensor was systematically characterized with various techniques including atomic force microscopy, gel electrophoresis, cyclic voltammetry, and electrochemical impedance spectroscopy, and its performance was optimized under a variety of experimental conditions especially the concentration of each reagent as well as its incubation time.

Under the optimal experimental conditions, the reported biosensor showed a very low limit of detection of 0.10 fM (S/N = 3) and a wide linear dynamic range covering from 0.50 fM to 100 pM towards microRNA-155, with excellent specificity, stability, and reproducibility. Finally, the biosensor was successfully applied to detect the amount of microRNA-155 extracted from the colon cancer cell line DLD1, demonstrating its potential applications in sensitive detection of biological samples in early diagnosis of diseases.

Keywords: ECL sensor, MicroRNA, Triplex DNA, HCR

INTRODUCTION

A microRNA (miRNA) is a type of endogenously expressed single-stranded, non-protein encoded RNA,[1] often with ~18-24 nucleotides that participate in the post-transcriptional regulation of gene expression.[2] Recent studies have shown that more than 30% of protein-coding genes may become target genes for miRNAs, and 50% of miRNAs are highly expressed in fragile sites in cancer-associated regions or gene expression.[3] Therefore, miRNAs have become clinically important biomarkers of early cancer diagnosis and prognosis, and their sensitive and selective analysis could certainly help us to understand some fundamental aspects of certain types of tumors by e.g., conducting relevant clinical research and drug efficacy evaluation.[4,5] A number of approaches have been reported in the literature for detection and quantification of miRNAs, which include methods based on biological nanopores,[6-8] electrochemistry,[9,10] fluorescence,[11-13] and electrogenerated chemiluminescence (ECL).[14-17] ECL is a combination of electrochemistry and photoluminescence, and offers unique advantages over its counterparts in quantitative analysis,[18] such as high sensitivity, wide detection range, good reproducibility, and low detection limit, as demonstrated by a series of comparison studies.[19-21]

Although ECL based biosensors hold great promise in detecting trace amounts of target species, fabrication of an ultrasensitive and robust biosensor with outstanding specificity towards the target still remains challenging. These challenges include (a) effective attachment of the target recognition element (probe) onto the electrode surface and its stability during the redox cycling, (b) accessibility of the target to the probe as well as efficient redox reactions of the ECL coreactant at the probe-target assembled electrode, (c) design and selection of the target specific probe, (d) signal reporting element (e.g., ECL emitter) that directly correlates the analytical signal to the target concentration, and (e) signal amplification mechanism. For example, to improve the

recognition abilities of surface-confined probes, much effort has been devoted to control the surface chemistry, conformation, and packing density of the probe molecules as well as the size and geometry of the surface.[22,23] By changing the probe attachment from the Au-S bonding to the C-N covalent coupling, an electrochemically stable and highly reusable ECL sensor for sensitive detection of cocaine was achieved.[24] Additionally, several strategies have been employed to enhance the signal intensities via, e.g., dramatically increasing the molar ratio of the ECL emitter to the target without affecting the bioactivities of the probe and target,[25-28] or in situ catalytically generating of the ECL coreactant.[29]

The present study attempts to construct an ECL based miRNA biosensor that addresses several of the aforementioned challenges. As will be described in details in the "Fabrication of the biosensor for detecting miRNA" section under EXPERIMENTAL SECTION, the proposed biosensor uses electrodeposited reduced graphene oxide on glassy carbon electrode (ERGO/GCE) as a substrate for the attachment of the probe bearing a triple-stranded DNA (tsDNA) nanostructure[30,31] in which three identical single-stranded DNA (ssDNA) tails (i.e., AAAA AAAA-) are dangled at one end and a miRNA specific ssDNA sequence is at the other end. The use of the ERGO provides not only a large active surface area for anchoring of the three tails via relatively strong π-π stacking[32-35] but also an excellent conductive interface for ECL coreactant redox reaction. Comparing with previously reported linear or stem-loop probe structures,[36] the present strategy employing triplex DNA nanostructured recognition probes on a surface could effectively avoid probe tangles and potential steric hindrance effect towards the subsequent reactions. In other words, the use of the triplex DNA platform may well improve the accessibility of the probes, resulting in effective coupling of the target molecules and enhancing the signal amplification efficacy. This could be attributed to the following two possible reasons:

First, the tripod structure is a highly rigid scaffold that accommodates DNA probes with well-defined probe-probe spacing and orientation. Second, the high binding affinity between the ssDNA tails and graphene but the poor affinity between triplex DNA and graphene, along with the relatively strong repulsion of negatively charged tripod probes, leads the tripod structure to stand up from the electrode surface. Given the fact that each of the three tails of the tripod has eight "A" bases, and the distance of each base-pair of dsDNA is ~0.34 nm and the length per base in ssDNA is ~0.68 nm,[37] it can be estimated that the tripod is spaced around 2.7 to 5.4 nm. To control DNA orientation as well as to provide sufficient space for target DNA hybridization, binary and ternary mixed self-assembled monolayers have been previously employed.[38] The obtained tsDNA/ERGO/GCE electrode is then treated with the target miRNA, and the probe ssDNA hybridizes with the complementary portion of miRNA. Signal amplification is accomplished on the basis of the subsequent hybridization chain reactions (HCR)[39,40] with two specifically designed hairpin DNA sequences, leading to the formation of an extended double helical DNA chain linked to the remaining portion of the miRNA. The ECL emitter $[Ru(bpy)_2(dppz)]^{2+}$ (bpy = 2,2′-bipyridine, dppz = dipyrido[3,2-*a*: 2′,3′-*c*]phenazine, Figure S1) is able to intercalate into the double-stranded DNA,[41] and produce ECL upon anodic potential scanning in the presence of an ECL coreactant such as tri-*n*-propylamine (TPrA). Because only $[Ru(bpy)_2(dppz)]^{2+}$ bonded to duplex DNA can produce efficient fluorescence[41,42] and ECL,[43] and weak emissions are given from its free form or residuals on the electrode, non-specific ECL emission causing high background signals is minimized. The above design principle was examined with the target analyte miRNA-155 from both a standard and a real biological sample. Unlike other miRNAs such as miRNA-21[9,10,12,13,15] and miRNA-141,[16] quantification of miRNA-155 has been seldom reported in the literature.

EXPERIMENTAL SECTION

Preparation of reduced graphene oxide modified electrode (ERGO/GCE). Reduced GO film was electrodeposited on GCE via cyclic voltammetry (CV).[44-46] The GCE was first polished with 0.05 μm alumina powder, followed by ultrasonication in ultrapure water and then anhydrous ethanol before it was dried with a stream of N_2. The cyclic voltammetric reduction was carried out in 0.10 mg/mL GO suspension in 0.10 M PBS (pH 7.4) under magnetic stirring and N_2 bubbling by cycling the electrode potential between -1.50 and 0.50 V vs Ag/AgCl for various cycles at a scan rate of 50 mV/s. The resulting electrode was washed with copious amounts of water and designated as ERGO/GCE. Upon electrodeposition, a grayish-dark layer was seen on GCE, and the film obtained from seven CV cycles displayed the optimal performance on miRNA sensing.

Synthesis of triple-stranded DNA (tsDNA).

To form a triplex DNA (tsDNA) structure, a double-stranded DNA (dsDNA) configuration was first created.[31] Briefly, 50 μL of 100 μM ssDNA-1 (Table S1) in 0.10 M PBS (pH 7.4) was mixed with 50 μL of 100 μM ssDNA-2 in 0.10 M PBS (pH 7.4). The mixture solution was subsequently incubated at 95 ºC for 5 minutes using a polymerase chain reaction (PCR) machine (BIO-RAD T100 Thermal Cycler) before the reaction solution was gradually cooled down at 2 ºC/min to room temperature (RT), resulting in the DNA hybridization and dsDNA formation. To the above solution, 100 μL of 50 μM ssDNA-3 in 0.10 M PBS (pH 7.4) and 200 μL of 10 mM $MgCl_2$ (i.e., the final $[Mg^{2+}]$ = 5 mM) were added, and the mixture was allowed to react at 4 ºC for 12 h to form a stable triple-stranded DNA (See Figure S4 for optimization of $[Mg^{2+}]$). The resultant solution containing the desired tsDNA of ~12.5 μM was stored at -20 ºC for later use.

Fabrication of the biosensor for detecting miRNA. A schematic representation of the

stepwise fabrication procedure for the proposed biosensor is shown in Scheme 1. A self-assembled monolayer of tsDNA was first formed on the ERGO/GCE by casting of 5 μL of the synthesized tsDNA on ERGO/GCE and allowing to incubate at RT for 40 min before it was thoroughly rinsed with 5 mM PBS (pH 7.4) and water. During this process, adsorption of the tsDNA onto the ERGO via π-π stacking interactions between the three dangled "AAAA AAAA-" bases and the graphene layer is expected, because single-stranded DNA can be adsorbed on reduced graphene oxide much stronger than double-stranded DNA.[32-35] As a result, the assembled tsDNA is likely to stand up on the electrode surface and does not require backfilling. The probe was like a tripod standing on the electrode surface. The resulting electrode is designated as tsDNA/ERGO/GCE. Afterwards, 10 μL aliquots of 0.10% DEPC aqueous solutions containing the target miRNA at various concentrations were placed on the modified electrode with incubation at RT for 60 min before washed with 5 mM PBS and water. Hybridization between the unbonded tail of ssDNA-3 and the complementary portion of miRNA-155 is expected to occur. The obtained electrode was further reacted with 10 μL of H_1-DNA and H_2-DNA mixture solution (5 μM each in 0.10 M PBS, pH 7.4) for 2 h to perform the effective hybridization chain reaction (HCR).[39,40] The newly formed double helical DNA chain was subsequently allowed to react with 10 μL of 30 μM Ru-dppz for 60 min, leading to robust binding of Ru-dppz complex to the DNA helix chain.[41] Note that all of the above incubation and hybridization reactions were carried out within a moisture-saturated plexiglass box. Finally, before the ECL measurements, which were conducted in 0.10 M TPrA-0.3 μM Ru-dppz-0.12 M PBS, the resulting functionalized electrode was thoroughly rinsed with 5 mM PBS and water.

RESULTS AND DISCUSSION

Characterization of GO and tsDNA/GO. Figure 1 shows the AFM images of (A) GO on

mica and (B) tsDNA on GO/mica, respectively. Clearly, GO nanosheets are well dispersed on mica with a height of ~1.3 nm (Figure 1A and Inset 1), suggesting that GO used in this study is a single layer.[47] The lateral size of GO nanosheets is estimated to be 100-200 nm. As shown in Figure 1B, after the treatment of GO/mica with tsDNA, white spots, which is an indication of tsDNA strongly adsorbed on the top of GO,[48] are seen. It is also evident that tsDNA cannot stick on mica (phyllosilicate) due to probably the lack of π-π interactions.[11] The height of tsDNA is estimated to be about 3~4 nm (Inset 2 of Figure 1), which is in good agreement with the length of the designed triple-stranded DNA structure (12 base-pairs, 0.34 nm/base-pair). This effectively proves that tsDNA vertically stands up on the top of GO. Thus, on ERGO/GCE, tsDNA should be also adsorbed in the form of vertical standing. This is because the binding of the tripod DNA on ERGO should be very similar to that on GO.

The feasibility of the miRNA detection strategy. The synthesis of tsDNA as well as the hybridization chain reaction (HCR) after the target miRNA was attached to the tsDNA were initially examined by polyacrylamide gel electrophoresis (PAGE). As shown in Figure 2A, the band of dsDNA (lane 1) resulting from ssDNA-1 and ssDNA-2 is located between that of ssDNA-3 (lane 2) and that of the tsDNA (lane 3), as the mobility (size) of the above three species follows an order of ssDNA-3 < dsDNA < tsDNA. In other words, tsDNA migrated the slowest (closest to the top of the panel) among the three. Under the present experimental conditions, no separate bands corresponding to either dsDNA or ssDNA-3 is seen in lane 3, confirming that tsDNA was synthesized efficiently. Lane 4 shows the result of an HCR reaction in solution, where equal moles (i.e., 5 μL×1.25 μM) of tsDNA and miRNA-155 were mixed with equal moles (i.e., 10 μL×5 μM) of H_1-DNA and H_2-DNA were used. As expected, a group of complexes are formed due to sequential HCR reactions, which reflects on a tailed band with slower mobility as

compared with that of tsDNA. Bands shown in lanes 5 and 6 are produced from H_1-DNA and H_2-DNA, respectively. The same number of bases and similar hairpin structure lead them to be appeared in the same position.

To further confirm the feasibility of the signal amplification strategy for target miRNA detection, ECL signals from different electrode surface configurations were recorded (Figure 2B). Curve a is the background ECL signal obtained from a tsDNA/ERGO/GCE, Curve b is the ECL response from the electrode of target miRNA/tsDNA/RRGO/GCE, and Curve c corresponds to the ECL signal of the proposed miRNA probe involving the use of the HCR strategy. A substantial increase in ECL intensity of ~3.4 times is achieved with the HCR reaction (Curve c vs Curve b), conforming our present HCR-based protocol indeed can amplify the ECL signal significantly. This is because one single target miRNA can only hybridize with one single capture probe of ssDNA-3 to form a 12-base pair long dsDNA, which limits the total number of Ru-dppz species intercalated into the double helix. In contrast, a much longer dsDNA hybrid structure can be formed via the designed HCR reaction, which enables many more Ru-dppz molecules to be intercalated into the dsDNA grooves with high affinity,[41] resulting in the amplification of ECL signal. Note that although electrodes with intercalated Ru-dppz could also generate ECL with the electrolyte containing anodic ECL coreactant TPrA, the addition of trace amounts of Ru-dppz (0.30 μM) to the electrolyte can considerably enhance the total ECL signal and provide a much better signal to noise ratio, due to probably the stabilization of the intercalated Ru-dppz with the Ru-dppz dissolved in solution. Additionally, the background ECL resulting from the nonspecific adsorption of Ru-dppz on thoroughly washed bare and DNA modified electrodes became well controlled. This approach was validated by our previous studies[49] and used in the electrochemical investigation of methylene blue at DNA modified electrode.[50]

Electrochemical characterizations of the biosensor. Cyclic voltammetry (CV) and electrochemical impedance spectroscopy (EIS) were performed to further explore the feasibility of the HCR-based biosensor. Figure 3A shows cyclic voltammograms (CVs) of $[Fe(CN)_6]^{3-/4-}$ from electrodes prepared at different stages of the biosensor. CVs at the bare GCE (Figure 3A(a)) and the ERGO/GCE (Figure 3A(b)) display nearly the same well-defined reversible responses with slightly larger peak currents and a smaller peak potential separation from the latter, suggesting that the electrochemically reduced graphene oxide film has good conductivity and a bit increased surface area (more evidence is given by EIS data shown below). These properties could make the ERGO film to be a sensitive promoter for electrochemical sensing.[51] The attachment of tsDNA (Figure 3A(c)), target miRNA/tsDNA (Figure 3A(d)), and H_1-DNA/H_2-DNA/miRNA/tsDNA (Figure 3A(f)) to the ERGO/GCE dramatically decreases the CV currents and increases the peak separation potentials, which can be readily explained using the electrostatic expelling effect between the negatively charged redox couple $[Fe(CN)_6]^{3-/4-}$ and the negatively charged DNA or RNA backbones. As the negative charge density of the electrode surface increases from tsDNA, to miRNA/dsDNA, to H_1-DNA/H_2-DNA/miRNA/tsDNA, their CV currents gradually decrease as expected. Note that the above changes in CV behavior should not be contributed to the changes in surface electrical resistance as a result of DNA or RNA hybridizations.[52]

The above CV observations are well consistent with the EIS data (Nyquist plots) illustrated in Figure 3B. All electrodes show a similar solution resistance that can be estimated from the Nyquist plot origin to the first intercept with the x-axis,[53,54] because the same redox media were used. However, the electron-transfer resistance (R_{et}), which can be estimated from the diameter of the semi-circle in the Nyquist plot, varies with the electrode surface configuration. Upon the

electrodeposition of ERGO onto the GCE, a decrease in R_{et} is observed (plot a vs plot b in Figure 3B, Inset), suggesting ERGO can promote the electron-transfer process. With the attachment of tsDNA to ERGO/GCE (Figure 3B(c)) and subsequent hybridization of target miRNA (Figure 3B(d)) and then the HCR reaction (Figure 3B(e)), the R_{et} value increases step-by-step, due to the repulsive electrostatic effect as discussed earlier. Both CVs and EIS spectra undoubtedly confirm the successful assembly of stepwise fabrication of the miRNA biosensor.

Optimization of experimental conditions. A number of factors that could affect the analytical performance of the miRNA biosensor were systematically examined, which include (a) the concentration of tsDNA on ERGO/GCE (Figure 4A) and its incubation time (Figure 4B), (b) concentrations of H_1-DNA and H_2-DNA used in the HCR (Figure 4C) and the HCR reaction time (Figure 4D), and (c) concentration of ECL emitter Ru-dppz (Figure 4E) and its incubation time (Figure 4F) in preparing of the ECL responsive RNA probe. Of course, when one parameter was investigated, the optimum conditions for others were used as described in the EXPERIMENTAL SECTION. The above three sets of data demonstrate a very similar trend, which is, with the increase of tested species concentration or the incubation (reaction) time of respective species, the ECL signal almost linearly increases until it levels off. The ultimate goal of these experiments is to find out under what conditions the fabricated biosensor could maximize the amounts of the ECL emitter Ru-dppz intercalated into the double helix of ssDNA-3/RNA as well as H_1-DNA/H_2-DNA chain, because the intercalated [Ru-dppz] is expected to be proportional to the target miRNA concentration as well as the ECL intensity.

On the basis of the above studies, the following optimal conditions were chosen for the fabrication of the RNA biosensor: C_{tsDNA} = 7 μM with an incubation time of 40 min, $C_{H_1\text{-DNA}}$ = $C_{H_2\text{-DNA}}$ = 5 μM with a HCR reaction time of 2 h, and $C_{Ru\text{-dppz}}$ = 30 μM with an incubation time of

60 min.

Analytical performance of the miRNA biosensor. Figure 5A shows the ECL responses under the CV scans of the RNA biosensor pre-treated with different concentrations of miRNA-155 (C_{RNA}), in which sensitive and yet distinguishable from the blank ECL signals are detected at $C_{RNA} \geq 0.50$ fM. With the increase of C_{RNA}, a steady increase in ECL response is observed. Figure 5B(a) shows the correlation between the ECL peak intensity and logC_{RNA} over a wide dynamic range of 0.50 fM to 1.0 μM, with a nonlinear curve fitting equation of y = 9101 - 763.5×logC_{RNA} - 74.68× (logC_{RNA})^2 (R^2 = 0.998, y = ECL peak intensity). Such a nonlinear calibration curve, in principle, could still be used for quantifying of unknown target miRNA-155-containing samples. A classical linear correlation is obtained within the lower C_{RNA} range of 0.50 fM to 100 pM (Figure 5B(b)), with a linear least squares fitting equation of y = 21566.3 + 1179.5×logC_{RNA} (R^2 = 0.992). The relative standard deviation (RSD) of the above set of data ranging from 0.8% to 8.3%, which is reflected on the relatively small error bars in Figure 5B, is an indication that the present RNA biosensor has good reproducibility. The limit of detection (LOD) is estimated to be 0.1 fM on the basis of LOD = 3σ/m (at 99.7% confidence level), where σ is the standard deviation of the response at low concentrations (or blank) and m is the slope of the calibration curve.[55,56] The deviation of the ECL intensity from the linearity at higher C_{RNA} (i.e., 1.0 nM to 1.0 μM, Figure 5B(a)) is probably due to the fact that formation of high density of the tsDNA/RNA duplex on the electrode surface sterically hinders the subsequent HCR reactions and thus limits the amounts of Ru-dppz complex intercalation.

Table S2 lists the comparison of eight different RNA biosensors using various detection methods and signal amplification or recognition strategies. High performance of the present RNA biosensor targeting miRNA-155 is evidently demonstrated with a relatively low LOD as well as a

wide linear dynamic range.

Selectivity, stability, and reproducibility of the RNA biosensor. As structurally similar RNAs, such as miRNA-21, miRNA-141 and miRNA-205, are often found to coexist in analytical samples, selective detection of a specific miRNA has become a great challenge.[57,58] Figure 6A shows the selectivity studies of our RNA biosensor by comparing the ECL peak values towards (a) blank, (b) miRNA-21 (10 pM), (c) miRNA-141 (10 pM), (d) miRNA-205 (10 pM), (e) miRNA-155 (1.0 pM), and (f) the mixture of (b)-(e), respectively. Each of the three tested potential interfering RNA sequences of miRNA-155 gives an ECL response similar to that of the blank. In contrast, the ECL intensity of the biosensor with only 1.0 pM target miRNA-155 displays a sharp increase (Figure 6A(e) vs 6A(a)-(d)). Furthermore, for a sample that contains the above three interfering agents (each at 10 pM) mixed with the target miRNA-155 (1.0 pM only), the detected ECL signal shows a value close to that of the miRNA-155 alone (Figure 6A(e) vs (f)). This set of comparison study undoubtedly demonstrates the high specificity of the proposed biosensor towards miRNA-155.

The stability study of the biosensor was conducted with 10 fM miRNA-155 under the optimal experimental conditions. As shown in Figure 6B, stable ECL signals are observed during a period of continuous 15 CV cycles between 0 and 1.40 V vs Ag/AgCl, with an RSD of 1.11%. Besides, three miRNA-155 biosensing electrodes were prepared in parallel using 1.0 pM target, and their ECL signals had an RSD of 4.51%. These data suggest that the present RNA biosensor holds significant stability and reproducibility.

Application of the proposed biosensor in detecting of RNA from cancer cells. The practical applicability of the designed biosensor was tested by detecting miRNA-155 in biological cell lysates of the colon cancer cell line DLD1. Figure 7 shows the ECL signals

associated with the number of the cells used for extracting miRNA-155, in which the increase in ECL intensity is proportional to the increase in cell numbers. Previous studies have shown that the elevated level of miRNA-155 could suggest the overexpression of miRNA-155 in DLD1 cells.[63,64] Therefore, the good feasibility in real sample analysis confirms that our proposed RNA biosensor holds great potentials in specifically and sensitively detecting miRNA-155 in biological samples, which is vital in many cases including early diagnosis of cancers.

CONCLUSIONS

Taking advantages of the tripod structure, we employed the triple-stranded DNA as the RNA capture probe so as to increase the reactivity and accessibility of RNA and HCR reactions after the tsDNA was assembled on the electrodeposited reduced graphene oxide on GCE. ECL signal amplification strategy was based on the miRNA-155 specific HCR reaction that could significantly increase the length of the double helix DNA structure, allowing more Ru-dppz species to be intercalated into the double-stranded DNAs, hence generating efficient ECL responses. The present biosensor demonstrated a very low LOD of 0.10 fM and a wide linear dynamic range covering from 0.50 fM to 100 pM towards miRNA-155, with excellent specificity, stability, and reproducibility. Potential applications of the biosensor could include sensitive detection of biological samples in early stages of diseases, as demonstrated in detecting miRNA-155 in colon cancer cells.

Supporting Information:

The Supporting Information is available free of charge on the ACS Publications website at DOI: XXX

Experimental section (Chemicals and Materials; Apparatus; Cell culture and total miRNA extraction), Chemical structure of $[Ru(bpy)_2(dppz)]^{2+}$ (Figure S1), Cyclic votammograms of GO

on GCE (Figure S2), Characterization of electrochemically reduced GO (ERGO) by XPS (Figure S3), the sequences of DNA and microRNA (Table S1), Comparison of the present work with previously reported miRNA detection methods (Table S2), and Optimization of [Mg^{2+}] on tsDNA hybridization (Figure S4).

Notes: The authors declare no competing financial interest.

ACKNOWLEDGEMENTS

This investigation was financially supported by the National Natural Science Foundation of China (No. 21527808, 21475006), Beijing municipal high level innovative team building program (IDHT 20180504) and the NSF CAREER Award (CHE 0955878, WJM).

REFERENCES:

(1) Dong, H.; Lei, J.; Ding, L.; Wen, Y.; Ju, H.; Zhang, X. Microrna: Function, detection, and bioanalysis, *Chem. Rev.* **2013**, *113*, 6207-6233.

(2) Bartel, D. P. MicroRNAs: Genomics, biogenesis, mechanism, and function, *Cell* **2004**, *116*, 281-297.

(3) Berezikov, E.; Guryev, V.; van de Belt, J.; Wienholds, E.; Plasterk, R. H. A.; Cuppen, E. Phylogenetic shadowing and computational identification of human microRNA genes, *Cell* **2005**, *120*, 21-24.

(4) Johnson, B. N.; Mutharasan, R. Biosensor-based microRNA detection: Techniques, design, performance, and challenges, *Analyst* **2014**, *139*, 1576-1588.

(5) Lee, J. M.; Jung, Y. Two-temperature hybridization for microarray detection of label-free microRNAs with attomole detection and superior specificity, *Angew. Chem. Int. Ed.* **2011**, *50*, 12487-12490.

(6) Zhang, J.-H.; Liu, X.-L.; Hu, Z.-L.; Ying, Y.-L.; Long, Y.-T. Intelligent identification of multi-level nanopore signatures for accurate detection of cancer biomarkers, *Chem. Commun.* **2017**, *53*, 10176-10179.

(7) Zhang, X.; Zhang, J.; Ying, Y.-L.; Tian, H.; Long, Y.-T. Single molecule analysis of light-regulated RNA:Spiropyran interactions, *Chemi. Sci.* **2014**, *5*, 2642-2646.

(8) Hu, Z.; Du, J.; Ying, Y.; Peng, Y.; Cao, C.; Long, Y.-T. Single-molecule analysis of colorectal cancer-associated MicroRNAs via a biological nanopore, *Acta Chim. Sinica* **2017**, *75*, 1087-1090.

(9) Su, S.; Cao, W.; Liu, W.; Lu, Z.; Zhu, D.; Chao, J.; Weng, L.; Wang, L.; Fan, C.; Wang, L. Dual-mode electrochemical analysis of microRNA-21 using gold nanoparticle-decorated MoS_2 nanosheet, *Biosens. Bioelectron.* **2017**, *94*, 552-559.

(10) Tian, L.; Qian, K.; Qi, J.; Liu, Q.; Yao, C.; Song, W.; Wang, Y. Gold nanoparticles superlattices assembly for electrochemical biosensor detection of microRNA-21, *Biosens. Bioelectron.* **2018**, *99*, 564-570.

(11) Huang, R.; Liao, Y.; Zhou, X.; Xing, D. Toehold-mediated nonenzymatic amplification circuit on graphene oxide fluorescence switching platform for sensitive and homogeneous microRNA detection, *Anal. Chim. Acta* **2015**, *888*, 162-172.

(12) Li, Y.; Pu, Q.; Li, J.; Zhou, L.; Tao, Y.; Li, Y.; Yu, W.; Xie, G. An "off-on" fluorescent switch assay for microRNA using nonenzymatic ligation-rolling circle amplification, *Microchim. Acta* **2017**, *184*, 4323-4330.

(13) Liu, C.; Lv, S.; Gong, H.; Chen, C.; Chen, X.; Cai, C. 2-aminopurine probe in combination with catalyzed hairpin assembly signal amplification for simple and sensitive detection of microRNA, *Talanta* **2017**, *174*, 336-340.

(14) Chen, A.; Ma, S.; Zhuo, Y.; Chai, Y.; Yuan, R. In situ electrochemical generation of electrochemiluminescent silver naonoclusters on target-cycling synchronized rolling circle amplification platform for microrna detection, *Anal. Chem.* **2016**, *88*, 3203-3210.

(15) Feng, Q.-M.; Shen, Y.-Z.; Li, M.-X.; Zhang, Z.-L.; Zhao, W.; Xu, J.-J.; Chen, H.-Y. Dual-wavelength electrochemiluminescence ratiometry based on resonance energy transfer between Au nanoparticles functionalized g-C_3N_4 nanosheet and $Ru(bpy)_3^{2+}$ for microRNA detection, *Anal. Chem.* **2016**, *88*, 937-944.

(16) Li, Z.; Lin, Z.; Wu, X.; Chen, H.; Chai, Y.; Yuan, R. Highly efficient electrochemiluminescence resonance energy transfer system in one nanostructure: Its application for ultrasensitive detection of microrna in cancer cells, *Anal. Chem.* **2017**, *89*, 6029-6035.

(17) Xiong, H.; Zheng, X. Electrochemiluminescence based determination of micro-RNA using target-guided assembly of gold nanoparticles on an electrode modified with Nafion, carbon nanotubes and polyvinylpyrrolidone, *Microchim. Acta* **2017**, *184*, 1781–1789.

(18) Miao, W. Electrogenerated chemiluminescence and its biorelated applications, *Chem. Rev.* **2008**, *108*, 2506-2553.

(19) Chowdhury, F.; Williams, A.; Johnson, P. Validation and comparison of two multiplex technologies, luminex® and mesoscale discovery, for human cytokine profiling, *J. Immunol. Methods* **2009**, *340*, 55-64.

(20) Fichorova, R. N.; Richardson-Harman, N.; Alfano, M.; Belec, L.; Carbonneil, C.; Chen, S.; Cosentino, L.; Curtis, K.; Dezzutti, C. S.; Donoval, B.; Doncel, G. F.; Donaghay, M.; Grivel, J.-C.; Guzman, E.; Hayes, M.; Herold, B.; Hillier, S.; Lackman-Smith, C.; Landay, A.; Margolis, L.; Mayer, K. H.; Pasicznyk, J.-M.; Pallansch-Cokonis, M.; Poli, G.; Reichelderfer, P.; Roberts, P.; Rodriguez, I.; Saidi, H.; Sassi, R. R.; Shattock, R.; Cummins, J. J. E. Biological and technical variables affecting immunoassay recovery of cytokines from human serum and simulated vaginal fluid: A multicenter study, *Anal. Chem.* **2008**, *80*, 4741-4751.

(21) Toedter, G.; Hayden, K.; Wagner, C.; Brodmerkel, C. Simultaneous detection of eight analytes in human serum by two commercially available platforms for multiplex cytokine analysis, *Clin. Vaccine Immunol.* **2008**, *15*, 42-48.

(22) Li, D.; Song, S.; Fan, C. Target-responsive structural switching for nucleic acid-based sensors, *Acc Chem Res* **2010**, *43*, 631-641.

(23) Ricci, F.; Zari, N.; Caprio, F.; Recine, S.; Amine, A.; Moscone, D.; Palleschi, G.; Plaxco, K. W. Surface chemistry effects on the performance of an electrochemical DNA sensor, *Bioelectrochemistry* **2009**, *76*, 208-213.

(24) Sun, B.; Qi, H.; Ma, F.; Gao, Q.; Zhang, C.; Miao, W. Double covalent coupling method for the fabrication of highly sensitive and reusable electrogenerated chemiluminescence sensors, *Anal. Chem.* **2010**, *82*, 5046-5052.

(25) Acharya, D.; Bastola, P.; Le, L.; Paul, A. M.; Fernandez, E.; Diamond, M. S.; Miao, W.; Bai, F. An ultrasensitive electrogenerated chemiluminescence-based immunoassay for specific detection of Zika virus, *Sci. Rep.* **2016**, *6*, 32227.

(26) Ma, F.; Zhang, Y.; Qi, H.; Gao, Q.; Zhang, C.; Miao, W. Ultrasensitive electrogenerated

chemiluminescence biosensor for the determination of mercury ion incorporating G4 PAMAM dendrimer and Hg(II)-specific oligonucleotide, *Biosens. Bioelectron.* **2012**, *32*, 37-42.

(27) Miao, W.; Bard, A. J. Electrogenerated chemiluminescence. 80. C-reactive protein determination at high amplification with $[Ru(bpy)_3]^{2+}$-containing microspheres, *Anal. Chem.* **2004**, *76*, 7109-7113.

(28) Miao, W.; Bard, A. J. Electrogenerated chemiluminescence. 77. DNA hybridization detection at high amplification with $[Ru(bpy)_3]^{2+}$-containing microspheres, *Anal. Chem.* **2004**, *76*, 5379-5386.

(29) Lu, L.; Liu, C.; Kang, T.; Wang, X.; Guo, G.; Miao, W. In situ enhanced electrochemiluminescence based on co-reactant self-generated for sensitive detection of microRNA, *Sensors Actuators B: Chem.* **2018**, *255*, 35-41.

(30) Casey, B. P.; Glazer, P. M. In *Progress in nucleic acid research and molecular biology*; Academic Press, 2001; Vol. 67, pp 163-192.

(31) Guntaka, R. V.; Varma, B. R.; Weber, K. T. Triplex-forming oligonucleotides as modulators of gene expression, *Int. J. Biochem. Cell Biol.* **2003**, *35*, 22-31.

(32) Lu, C.; Huang, P.-J. J.; Liu, B.; Ying, Y.; Liu, J. Comparison of graphene oxide and reduced graphene oxide for DNA adsorption and sensing, *Langmuir* **2016**, *32*, 10776-10783.

(33) Wang, Y.-H.; Deng, H.-H.; Liu, Y.-H.; Shi, X.-Q.; Liu, A.-L.; Peng, H.-P.; Hong, G.-L.; Chen, W. Partially reduced graphene oxide as highly efficient DNA nanoprobe, *Biosens. Bioelectron.* **2016**, *80*, 140-145.

(34) Yang, Y.; Asiri, A. M.; Tang, Z.; Du, D.; Lin, Y. Graphene based materials for biomedical applications, *Mater. Today* **2013**, *16*, 365-373.

(35) Yardım, Y.; Vandeput, M.; Çelebi, M.; Şentürk, Z.; Kauffmann, J. M. A reduced graphene oxide-based electrochemical DNA biosensor for the detection of interaction between cisplatin and DNA based on guanine and adenine oxidation signals, *Electroanalysis* **2017**, *29*, 1451-1458.

(36) Fan, C.; Plaxco, K. W.; Heeger, A. J. Electrochemical interrogation of conformational changes as a reagentless method for the sequence-specific detection of DNA, *Proc. Nat. Acad. Sci.* **2003**, *100*, 9134-9137.

(37) Chi, Q.; Wang, G.; Jiang, J. The persistence length and length per base of single-stranded DNA obtained from fluorescence correlation spectroscopy measurements using mean field theory, *Physica A* **2013**, *392*, 1072-1079.

(38) Dharuman, V.; Chang, B. Y.; Park, S. M.; Hahn, J. H. Ternary mixed monolayers for simultaneous DNA orientation control and surface passivation for label free DNA hybridization electrochemical sensing, *Biosens. Bioelectron.* **2010**, *25*, 2129-2134.

(39) Bi, S.; Yue, S.; Zhang, S. Hybridization chain reaction: A versatile molecular tool for biosensing, bioimaging, and biomedicine, *Chem. Soc. Rev.* **2017**, *46*, 4281-4298.

(40) Evanko, D. Hybridization chain reaction, *Nat. Methods* **2004**, *1*, 186.

(41) Friedman, A. E.; Chambron, J. C.; Sauvage, J. P.; Turro, N. J.; Barton, J. K. A molecular light switch for DNA: $Ru(bpy)_2(dppz)^{2+}$, *J. Am. Chem. Soc.* **1990**, *112*, 4960-4962.

(42) Zeglis, B. M.; Pierre, V. C.; Barton, J. K. Metallo-intercalators and metallo-insertors, *Chem. Commun.* **2007**, 4565-4579.

(43) Xiong, Y.; Kang, T.-F.; Lu, L.-P. Electrochemistry of complex formation of carbaryl with ds-DNA using $[Ru(bpy)_2dppz]^{2+}$ as probe, *J. Solid State Electrochem.* **2013**, *17*, 129-136.

(44) Chen, L.; Tang, Y.; Wang, K.; Liu, C.; Luo, S. Direct electrodeposition of reduced graphene oxide on glassy carbon electrode and its electrochemical application, *Electrochem. Commun.* **2011**, *13*, 133-137.

(45) Liu, C.; Wang, K.; Luo, S.; Tang, Y.; Chen, L. Direct electrodeposition of graphene enabling the one-step synthesis of graphene–metal nanocomposite films, *Small* **2011**, *7*, 1203-1206.

(46) Li, J.; Lu, L.; Kang, T.; Cheng, S. Intense charge transfer surface based on graphene and thymine-Hg(II)-thymine base pairs for detection of Hg^{2+}, *Biosens. Bioelectron.* **2015**, *77*, 740-745.

(47) Warner, J. H.; Schäffel, F.; Bachmatiuk, A.; Rümmeli, M. H. In *Graphene*; Elsevier, 2013, pp 229-332.

(48) Lu, C. H.; Yang, H. H.; Zhu, C. L.; Chen, X.; Chen, G. N. A graphene platform for sensing biomolecules, *Angew. Chem. Int. Ed.* **2009**, *48*, 4785-4787.

(49) Lu, L.; Wu, J.; Li, M.; You, X.; Kang, T.; Cheng, S. A bis(2,2′-bipyridine) (dipyrido[3, 2-a:2′ 3′-c]phenazine-N_4N_5) ruthenium(II)-based electrochemiluminescence biosensor for evaluation of DNA damage, *Anal. Lett.* **2015**, *48*, 116-126.

(50) Kelley, S. O.; Barton, J. K.; Jackson, N. M.; Hill, M. G. Electrochemistry of methylene blue bound to a DNA-modified electrode, *Bioconj. Chem.* **1997**, *8*, 31-37.

(51) Pumera, M. Electrochemistry of graphene: New horizons for sensing and energy storage, *Chem. Rec.* **2009**, *9*, 211-223.

(52) Pittman, T. L.; Miao, W. Examination of electron transfer through DNA using electrogenerated chemiluminescence, *J. Phys. Chem. C* **2008**, *112*, 16999-17004.

(53) Lu, L.; Guo, L.; Li, M.; Kang, T.; Cheng, S.; Miao, W. Investigation of perfluorooctanoic acid induced DNA damage using electrogenerated chemiluminescence associated with charge transfer in DNA, *Anal. Bioanal. Chem.* **2016**, *408*, 7137-7145.

(54) Chang, B.Y.; Park, S.M. Electrochemical impedance spectroscopy, *Annu. Rev. Anal. Chem.* **2010**, *3*, 207-229.

(55) Little, T. Method validation essentials, limit of blank, limit of detection, and limit of quantitation, *BioPharm Int.* **2015**, *28*, 48-51.

(56) Long, G. L.; Winefordner, J. D. Limit of detection a closer look at the IUPAC definition, *Anal. Chem.* **1983**, *55*, 712A-724A.

(57) Strubberg, A. M.; Madison, B. B. MicroRNAs in the etiology of colorectal cancer: Pathways and clinical implications, *Dis. Models & Mechanisms* **2017**, *10*, 197-214.

(58) Zhu, J.; Wang, S.; Zhang, W.; Qiu, J.; Shan, Y.; Yang, D.; Shen, B. Screening key microRNAs for castration-resistant prostate cancer based on mirna/mRNA functional synergistic network, *Oncotarget* **2015**, *6*, 43819-43830.

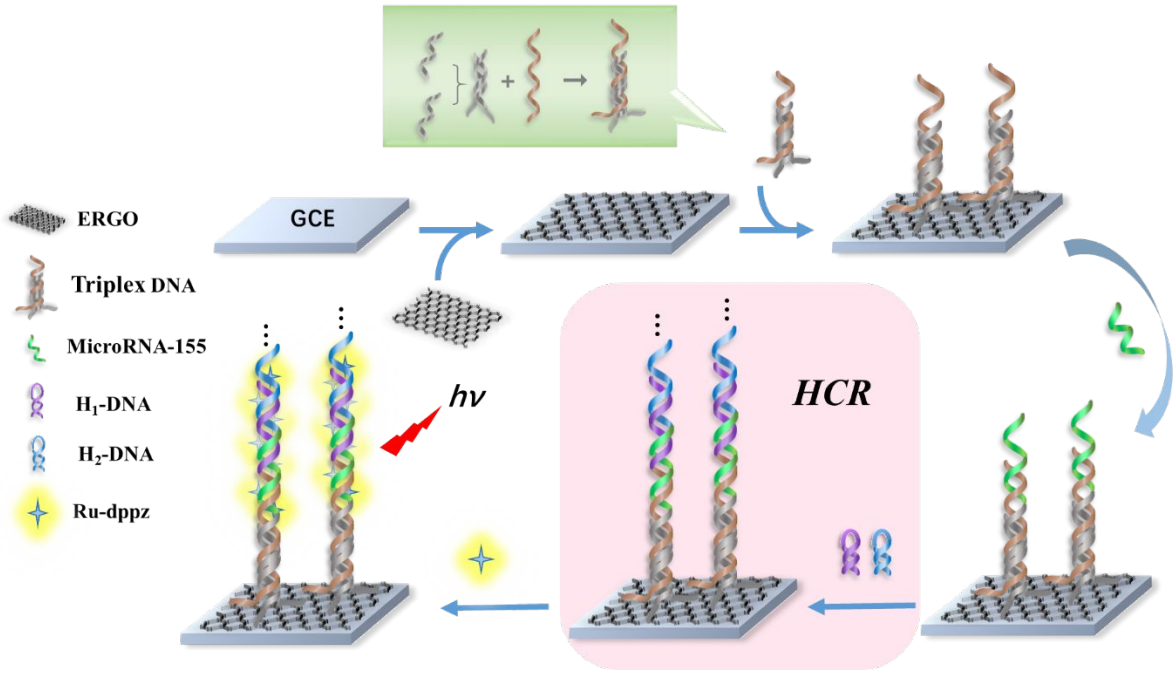

Scheme 1. Schematic representation of the stepwise ECL biosensor fabrication.

Figures and Captions

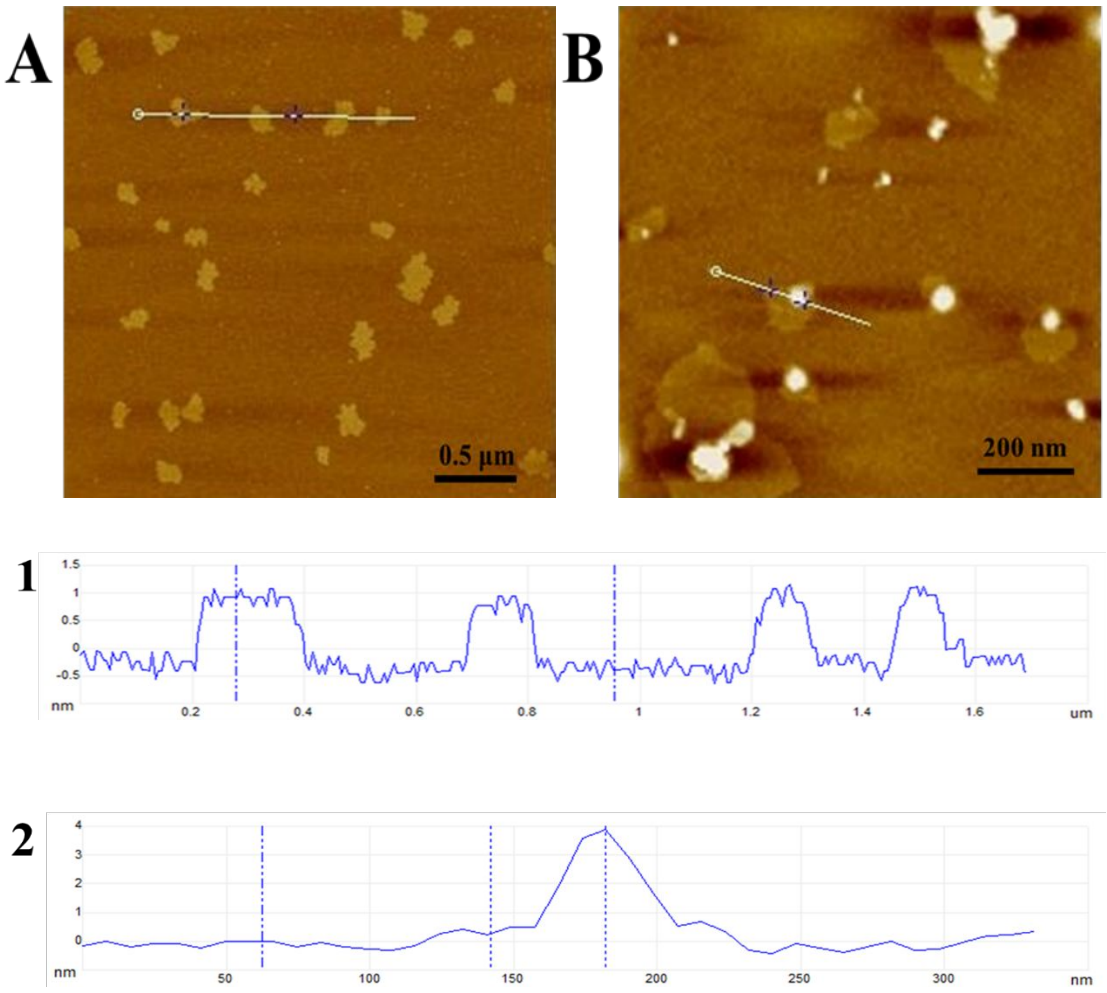

Figure 1. AFM images of (A) GO nanosheets and (B) tsDNA/GO on mica. The section profiles of the GO nanosheets and tsDNA/GO/mica along the dashed lines are shown in Insets 1 and 2, respectively.

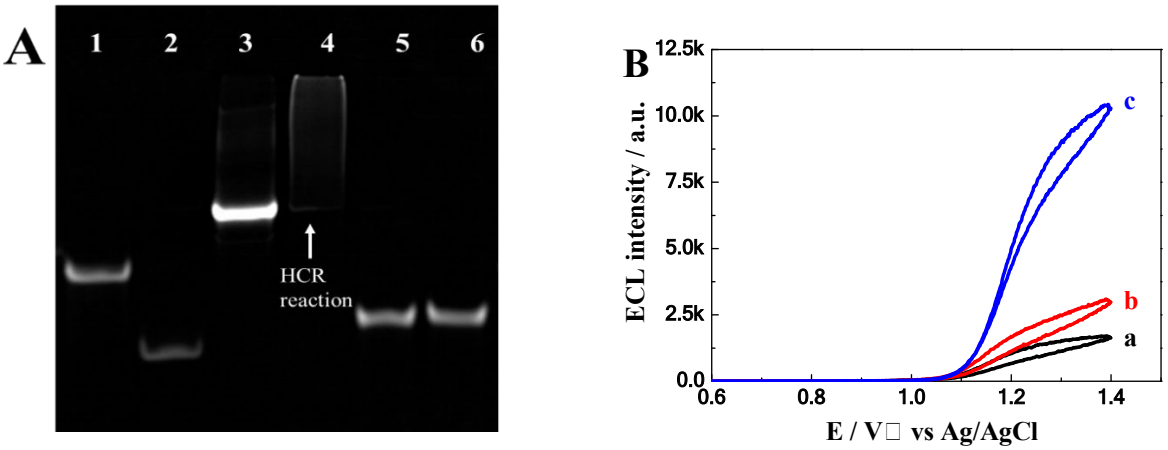

Figure 2. (A) Agarose gel electrophoresis demonstration of tsDNA and hybridization chain reaction (HCR): lane 1, hybrid of ssDNA-1 and ssDNA-2; lane 2, ssDNA-3; lane 3, tsDNA originated from ssDNA-1, 2, and 3; lane 4, hybrids of HCR reaction in solution, where equal moles (i.e., 5 μL×1.25 μM) of tsDNA and miRNA-155 were mixed with equal moles (i.e., 10 μL×5 μM) of H_1-DNA and H_2-DNA with the HCR reaction for 3 h; lane 5, H_1-DNA; lane 6, H_2-DNA. (B) ECL-potential profiles obtained from electrodes of tsDNA/ERGO/GCE, (b) target microRNA-155/tsDNA/ERGO/GCE, and (c) H_1-DNA/H_2-DNA/miRNA/tsDNA/ERGO/GCE. All of the three electrodes were pre-incubated with excess amounts of Ru-dppz. The ECL experiments were conducted in 0.10 M TPrA-0.30 μM Ru-dppz-0.12 M PBS (pH 7.5) at a scan rate of 50 mV/s.

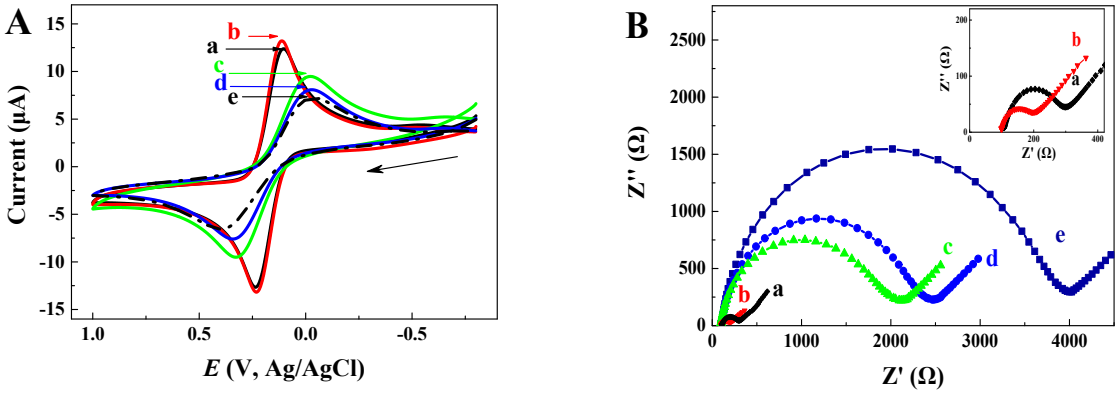

Figure 3. (A) CVs and (B) EIS spectra (Nyquist plots) of (a) GCE, (b) ERGO/GCE, (c) tsDNA/ERGO/GCE, (d) miRNA-155/tsDNA/ERGO/GCE, and (e) H_1-DNA/H_2-DNA/miRNA-155/tsDNA/ERGO/GCE. Experiments were conducted in 5.0 mM $K_3Fe(CN)_6$-5.0 mM $K_4Fe(CN)_6$ mixture containing 0.10 M KCl electrolyte at (A) 50 mV/s and (B) the formal redox potential, 0.20 V vs Ag/AgCl, of the $K_3Fe(CN)_6/K_4Fe(CN)_6$ system.

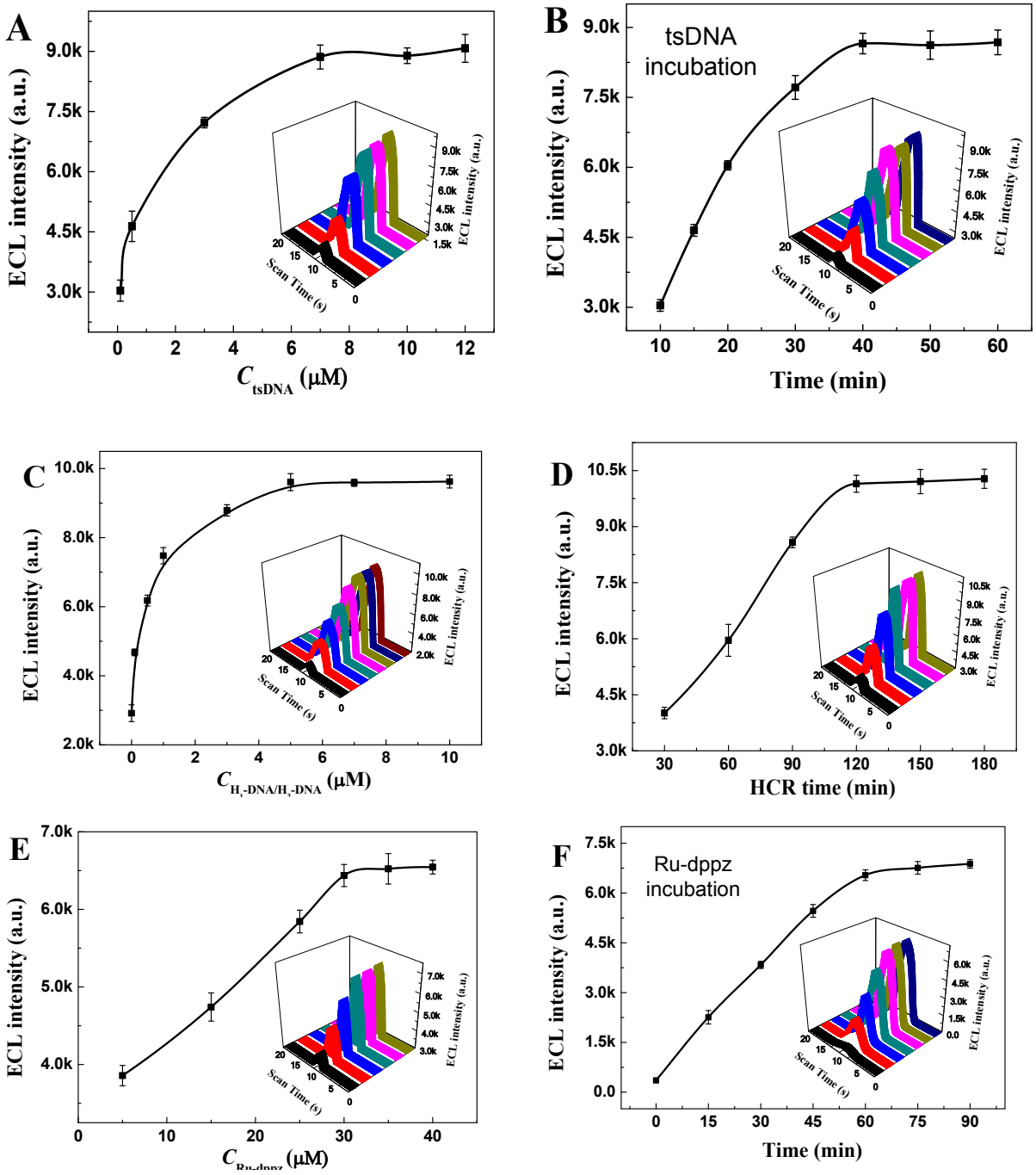

Figure 4. Dependence of ECL intensity of the miRNA biosensor on (A) tsDNA concentration and (B) its incubation time, (C) H_1-DNA/H_2-DNA concentrations and (D) the HCR reaction time, and (E) Ru-dppz concentration used in DNA incubation and (F) its incubation time. ECL experiments were conducted in 0.10 M TPrA-0.30 μM Ru-dppz-0.12 M PBS (pH 7.5) at a scan rate of 50 mV/s.

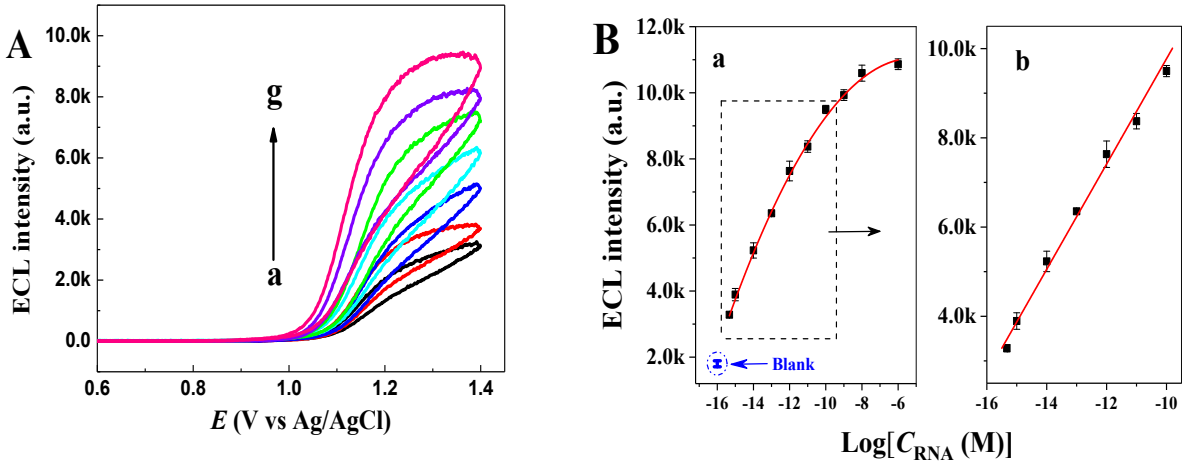

Figure 5. (A) ECL intensity vs potential profiles of the RNA biosensor in the presence of different concentrations of miRNA-155: (a) 0.5 fM, (b) 1.0 fM, (c) 10.0 fM, (d) 100.0 fM, (e) 1.0 pM, (f)10 pM, and (g) 100 pM. (B) The relationship between ECL peak intensity and miRNA concentration over a range of (a) 0.5 fM to 1.0 μM, and (b) 0.5 fM to 100 pM with linear regression. ECL experiments were carried out in 0.10 M TPA containing 0.12 M PBS (pH 7.5) and 0.30 μM Ru-dppz at a scan rate of 50 mV/s. The error bars represent the standard deviation of three repeated measurements.

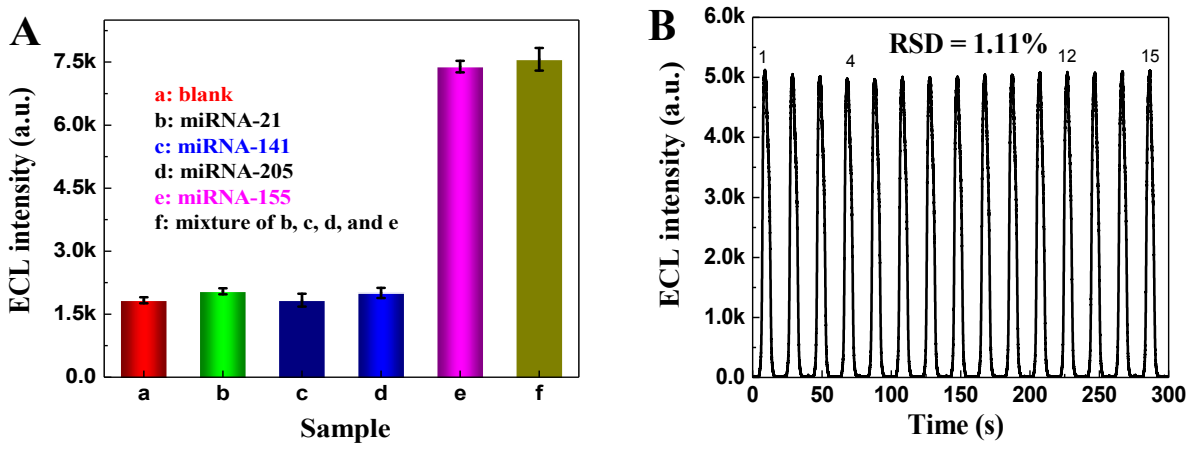

Figure 6. (A) Specificity of the miRNA biosensor: (a) blank, (b) miRNA-21 (10 pM), (c) miRNA-141 (10 pM), (d) miRNA-205 (10 pM), (e) miRNA-155 (1.0 pM), (f) mixture of miRNA-155 (1.0 pM), miRNA-21 (10 pM), miRNA-205 (10 pM), and miRNA-155 (10 pM). (B) Stability of the miRNA biosensor with consecutive cyclic potential scans for 15 cycles under optimal experimental conditions.

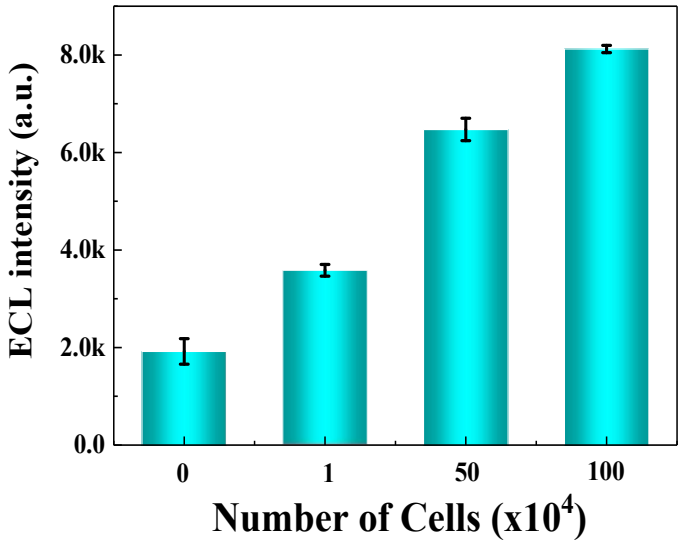

Figure 7. Detection of miRNA-155 from colon cancer line DLD1 lysates.

For TOC Only